STM JOURNALS

Journal of
Modern Chemistry &
Chemical Technology

ISSN: 2229-6999 (Online)
ISSN: 2321-5208 (Print)
Volume 16, Issue 2, 2025
May–August
DOI (Journal): 10.37591/JoMCCT

https://journals.stmjournals.com/jomcct

Review JoMCCT

Synthesis, Spectroscopic, Crystal Structure, Hirshfeld Surface, Computational, and Biological Investigations on Isophorone Derivatives: 3-(3,4-dimethoxystyryl)-5,5-dimethylcyclohex-2-en-1-one

M. Raj Kumar[1], U. Rajapandiyan[1], H. Manikandan[2,*], B. Premalatha[3], V. Rajathi[4], J. Arikrishnan[5]

Abstract

FT-IR, ^{1}H NMR, and ^{13}C NMR spectroscopy were among the spectroscopic methods used to synthesize and analyze 3-(3,4-dimethoxystyryl)-5,5-dimethylcyclohex-2-en-1-one, a new isophorone derivative. Single-crystal X-ray diffraction (SCXRD) was used to determine the crystal structure, which showed that the molecule crystallizes in a monoclinic system (space group P121/c1) with packing configurations and intermolecular interactions. To learn more about the non-covalent interactions influencing the crystal packing, Hirshfeld surface analysis was used. In order to analyse the electronic structure, molecular orbitals (HOMO-LUMO), RDG scatter diagram and scatter graph, Topological ELF, LOL parameters, and stability of the molecule, Density Functional Theory (DFT) calculations were carried out at B3LYP level 6-31G(d,p) basis set. Additionally, the synthetic compound's biological potential was assessed using its anti-inflammatory, anti-oxidant, and anti-diabetic properties, which showed encouraging action.

Keywords: Isophorone, Single Crystal X-RD, Computational Studies, Anti-diabetic, Anti-inflammatory Antioxidant.

***Author for Correspondence**
H. Manikandan
E-mail: profmani.au@mail.com

[1]Research Scholar, Department of Chemistry, Annamalai University, Annamalainagar, Tamil Nadu, India.
[2]Professor, Department of Chemistry, Annamalai University, Annamalainagar 608002, Tamil Nadu, India.
[3]Assistant Professor, Research Scholar, PG & Research Department of Chemistry, Government Arts College, Chidambaram, Tamil Nadu, India.
[4]Associate Professor Professor, Government Arts College, C Mutlur, Chidambaram, Tamil Nadu, India.
[5]Assistant Professor, Department of Chemistry, Rajalakshmi Engineering College, Thandalam, Chennai, Tamil Nadu, India

Received Date: May 02, 2025
Accepted Date: April 04, 2025
Published Date: August 23, 2025

Citation: M. Raj Kumar, U. Rajapandiyan, H. Manikandan, B. Premalatha, V. Rajathi, J. Arikrishnan. Synthesis, Spectroscopic, Crystal Structure, Hirshfeld Surface, Computational, and Biological Investigations on Isophorone Derivatives: 3-(3,4-dimethoxystyryl)-5,5-dimethylcyclohex-2-en-1-one. Journal of Modern Chemistry & Chemical Technology. 2025; 16(2): 51–69p.

INTRODUCTION

In synthetic organic chemistry, α, β-unsaturated carbonyl molecules are crucial intermediates, and several synthesis techniques have been documented so far. By reacting aromatic aldehydes with acidic carbonyl moieties, the most practical technique for creating α, β-unsaturated carbonyl systems is the mixed aldol reaction, often referred to as the Claisen-Schmidt condensation. To increase the synthetic range of this condensation process, a number of advancements have been developed in recent years [1].

Isophorone (3,5,5-trimethylcyclohex-2-en-1-one) is an α, β-unsaturated cyclic ketone widely used in industrial applications due to its unique chemical properties. It is a colorless to pale yellow liquid with a characteristic peppermint-like odor and is highly soluble in organic solvents. Isophorone is primarily utilized as a solvent in coatings, adhesives, printing

inks, and pesticides [2]. Despite its industrial applications, isophorone has garnered attention for its biological significance. Some studies suggest that isophorone and its derivatives exhibit potential candidates for pharmaceutical and agricultural applications. Additionally, its role in organic synthesis contributes to the development of bioactive compounds used in medicinal chemistry. However, further research is required to fully understand its potential benefits and mechanisms of action within biological systems. Moreover, its toxicological profile highlights the need for careful handling to minimize adverse health effects while exploring its possible therapeutic applications.

Diabetes mellitus is a well-known metabolic disorder that has become a serious problem of modern society due to severe long-term health complications associated with it [3]. It is a chronic, non-communicable metabolic disease categorized by acquired deficiency of insulin secretion and by decrease receptiveness of an organ to secrete insulin [4]. Glucose metabolism disturbances are major factors leading to diabetes. According to the estimated WHO report (2018), about 90% patients suffering from diabetes are diagnosed for type 2 DM. The breakdown of starch or glycogen into short chain monomer maltose is catalysed by the hydrolysing enzyme α-amylase (α-1,4-glucan-4-glucanohydrolases) which is secreted from pancreas, the maltose is further hydrolysed into glucose molecules by α-glucosidase enzyme. International Diabetes Federation in their study estimated that approximately 366 million people are having diabetes. Globally, the prevalence of diabetes and associated risks continues to increase and the number of patients with diabetes is expected to double up by 2030[5]. Antioxidants have gained attention due to their possible preventive and therapeutic properties against a variety of disorders. Free radicals are continuously produced as a result of regular organ processes or severe oxidative stress [6]. High amounts of free radicals can damage biomolecules including lipids, proteins, enzymes, and DNA in cells and tissues, causing mutations that can lead to cancer. The discovery of synthetic molecules capable of scavenging free radicals has been highly successful[7]. Inflammation is a dynamic reaction of the body to an external factor that disrupts its natural balance, usually pathogenic microbes or physical agents [8]. This procedure most often helps to eliminate the cause of tissue damage, but in other diseases, the body's response is insufficient. Prolonged inflammation may cause tissue damage, cellular destruction, or even accelerate the development of cancer. In addition to discomfort, heat, and loss of function, localized redness and swelling are the most common first signs of inflammation. Protein denaturation has been put forward as the source of the inflammation. Novel structures that may be implemented for the development of potent, less harmful anti-inflammatory drugs are becoming more and more necessary [9]. In general, finding the trifecta of efficacy, potency, and minimum unwanted effects is not always achievable, even though there are a number of therapies that help with the inflammatory disease. This is the reason why it is still crucial to look for new anti-inflammatory molecules while simultaneously looking for compounds that might lessen the oxidative processes that cause inflammation.

The current work aims to evaluate the structural features of an isophorone derivative (IPV). We reported that the synthesis process, single crystal X-ray structure, IR and NMR spectrum analysis findings, and theoretical assessments on the structures were carried out utilizing Density Functional Theory (DFT). To learn about the chemical reactivity properties of the compound, frontier molecular orbital energies, ionization potential, electron affinity, electronegativity, chemical hardness-softness, electronic structure parameters, topological ELF, LOL parameters, and RDG scatter diagram were examined at gas phase. In addition, anti-oxidant, anti-diabetic, and anti-inflammatory properties were studied.

EXPERIMENTAL

General

The experiment was executed using commercially obtained chemicals and reagents that were exempt from purification. The Agilent resolution Carry 630 was used to record FT-IR spectra in the 4000–400 cm^{-1} range utilizing the KBr disc method. With a spectral resolution of 8.0 cm^{-1}, the spectrum was captured at ambient temperature. Carbon NMR spectra were reported at 125.75 MHZ, whereas proton NMR spectra were recorded on a BRUCKER AVANCE 111 spectrometer running at 400 MHZ. About

10 mg of the chemical was dissolved in 0.5 ml of chloroform-d to develop the samples. Parts per million (ppm) of chemical changes in relation to internal TMS (0 ppm) were reported.

Synthesis

In a 250 ml round-bottom flask, isophorone (1.0 mmol) and 3,4-dimethoxybenzaldehyde (1.0 mmol) were dissolved in 50 ml of absolute ethanol. To this solution, sodium ethoxide (0.1 mmol) was added as a base. The reaction mixture was stirred at room temperature for 6 hours **(Scheme 1).** Upon completion, the reaction was quenched with water and the organic layer extracted with dichloromethane (DCM). The organic phase was dried over anhydrous sodium sulfate, filtered, and the solvent was removed under reduced pressure to yield the crude product. The crude product was purified by column chromatography using silica gel as the stationary phase and a mixture of hexane and ethyl acetate (4:1) as the eluent. The purified product was obtained as a yellow solid.

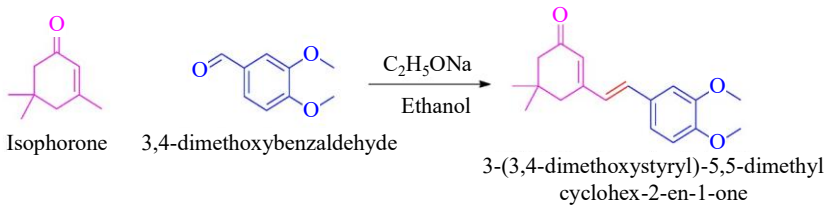

Isophorone 3,4-dimethoxybenzaldehyde 3-(3,4-dimethoxystyryl)-5,5-dimethyl cyclohex-2-en-1-one

Scheme 1. Synthetic route of 3-(3,4-dimethoxystyryl)-5,5-dimethylcyclohex-2- en-1-one (IPV).

Crystallography

The solvent evaporation method was used for the growth of high-quality single crystals suitable for an X-ray study. A slow evaporation of the solvent led to the formation of the yellow block-like crystal. The crystal data for the compound was collected on a Bruker D8 Quest instrument with a Photon detector and graphite-monochromated MoK radiation (λ=0.71073 A) at ambient temperature, 295 K. Data were corrected for absorption effects using the Multi-Scan method (SADABS). The structure was solved and refined using the Bruker SHELXTL software. The compound crystallized in monoclinic. Unit cell parameters are as follows: a = 23.041(7) Å, b = 5.9791(19) Å, c = 11.743(3) Å: α = 90°, β = 90.744(9)°, γ = 90°, with a space group P 1 21/c 1.

Computational Studies

The theoretical simulations were carried out using the GAUSSIAN 09W software programme. The density functional group theory (DFTB3LYP) technique was used to build the geometry with a 6-31G (d,p) basis set. The ideal structure of the molecules was shown using the molecular visualisation tool GAUSSVIEW5.0 [10]. The HOMO and LUMO energies as well as the Molecular Electrostatic Potential (MEP), Global Chemical Reactivity Descriptors (GCRD) [11] and Mulliken charges have all been calculated [12].

Biological Investigation

α-amylase Inhibition Technique

The samples' anti-diabetic activity was assessed using the α-amylase inhibition technique. Amylase (0.2%) was incubated with and without samples (1.5 ml) and standard for 10 minutes at 25°C. This experiment was carried out in 0.2 M phosphate buffer (pH 6.9). After pre-incubation, add the 1% starch solution (0.5 ml) and incubate at 25°C for 30 minutes. To stop the enzymatic reaction, 0.5 ml of DNSA reagent (color reagent) was added and incubated in a boiling water bath for 90 minutes. After cooling to room temperature, 0.5 ml of samples were diluted in 2.5 ml of distilled water and analyzed at 540 nm with a UV-Visible spectrophotometer. The measured absorbance was compared to that of the control experiment. The percentage inhibition was computed using the provided formula.

% of Inhibition = 100 x[Ac-At /Ac]

At: Absorbance of test, Ac: Absorbance of control

BSA Denaturation Technique

The produced drug and standard diclofenac sodium were tested for anti-inflammatory activity utilizing the inhibition of albumin denaturation approach, with minor modifications. The standard substance and product were dissolved in a small amount of dimethyl formamide (DMF) and diluted with phosphate buffer (0.2 M, pH 7.4). The final DMF concentration in all solutions was less than 2.5%. Test Solution (2.5 ml) containing various drug concentrations was combined with 1 ml of 1 mm Bovine serum albumin solution in phosphate buffer and incubated in an incubator at 37 °C for 10 minutes. Denaturation was induced by heating the reaction mixture in a water bath at 70°C for 10 minutes. After cooling, turbidity was measured at 660 nm. The percentage of denaturation inhibition was calculated from the control group that wasn't given any drugs. The percentage inhibition of denaturation was estimated using the procedure below.

% of Inhibition = 100 x[Ac-At /Ac]

At: Absorbance of test, Ac: Absorbance of control

Total Antioxidant Activity

The total antioxidant activity of the samples was evaluated. The test samples received approximately 3 ml of antioxidant reagent (0.6 M H_2SO_4, 28 mm Na_3PO_4, and 4 mm ammonium molybdate) at varying doses. To ensure proper diffusion with phosphomolybdenum reagent, the test mixture was incubated at 95°C in a water bath for 90 minutes. A spectrophotometer was used to assess the overall antioxidant activity of extracts and vitamin C standard drugs, as well as their absorbance at 695 nm. The total antioxidant activity were determined using the provided formula.

TOA = [(At−Ac) /At]X 100.

RESULTS AND DISCUSSIONS

Structural Characterization

An Isophorone derivative (IPV) was produced in high to outstanding yields from the efficient Claisen-Schmidt condensation process of isophorone and 3,4-dimethoxybenzaldehyde. The process initiates when sodium ethoxide deprotonates aldehyde to create the enolate. This enolate forms the IPV by nucleophilically attacking the isophorone's carbonyl atom after the water is removed. Using FT-IR spectroscopy, ^{1}H-NMR, and ^{13}C-NMR, the final product was described. The existence of the conjugated ketone was supported by the substantial carbonyl stretch in the IR spectra (Figure 1), which was seen at about 1650 cm^{-1}. At 1580 cm^{-1}, the aliphatic C=C stretching frequency was detected. The aliphatic C-H stretching frequency absorption band appears at 2952 cm^{-1} listed in Table 1. These spectroscopic findings corroborated the mechanism of the reaction, which involves the production of enolate and the following nucleophilic attack on isophorone.

The comparatively electron-rich environment of the two methyl protons causes them to show up as singlets in the upfield region (1.03 ppm). The two methoxy protons exhibit a singlet at 3.83 ppm –3.86 ppm, whereas the two methylene protons resonant at 2.23 ppm and 2.40 ppm, respectively. In 6.69 ppm -7.19 ppm, the aromatic protons show up as multiplets. The proton next to the carbonyl group is the reason for the singlet at 5.99 ppm were seen in the ^{1}H-NMR spectrum (Figure 2).

In ^{13}C NMR, (Figure 3) the two methyl groups attached to the cyclohexanone ring resonate at 28.53 ppm, whereas the two methoxy carbon signals show up at 55.94 ppm and 55.94 ppm. The positions of the olifinic carbons are 129.09 ppm and 134.99 ppm. The signal at 200.20 ppm is from carbonyl carbon. The range of aromatic carbons is 109.14 ppm to 155.08 ppm.

Diffractional studies

The single crystal x-ray diffraction technique verified the structure, which was then solved using the direct approach implemented in SHELXT 2014/5 [13]. SHELXL-2018/3 was used to refine the entire

matrix least-square of all non-hydrogen atoms [14]. With a maximum θ angle of 30.21° (0.71 Å resolution),

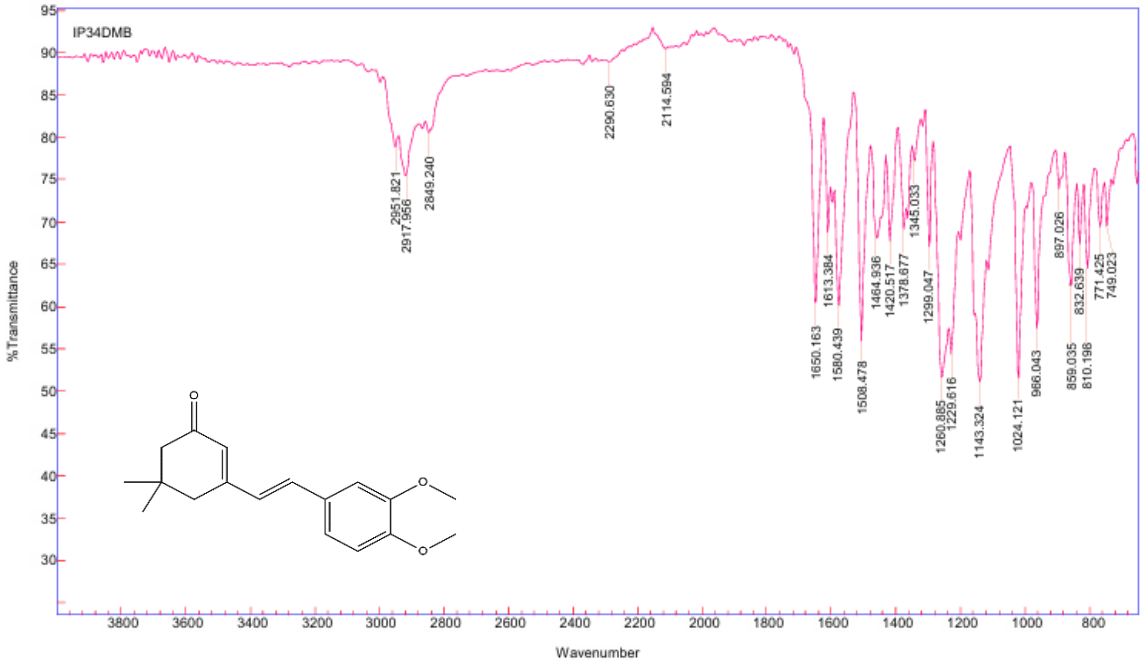

Figure 1. FT-IR spectrum of compound IPV.

Table 1. FT-IR spectral value (Cm^{-1}) of IPV

Assignment	Wave number
ν (C-H, a)	2950
ν (C =O, s)	1650
ν (C–O–C)	1260
ν (C–C, s)	1464
ν (C =C, s)	1580
δ (C–H) of –C(OCH3)2	1378

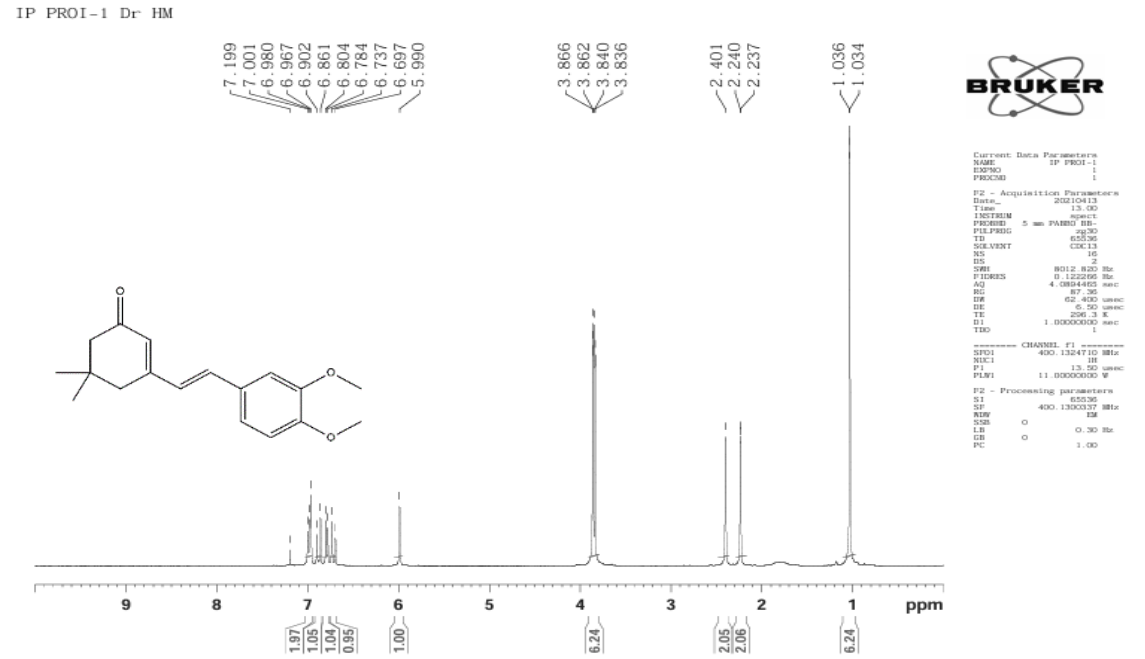

Figure 2. ^{1}H NMR spectrum of compound IPV.

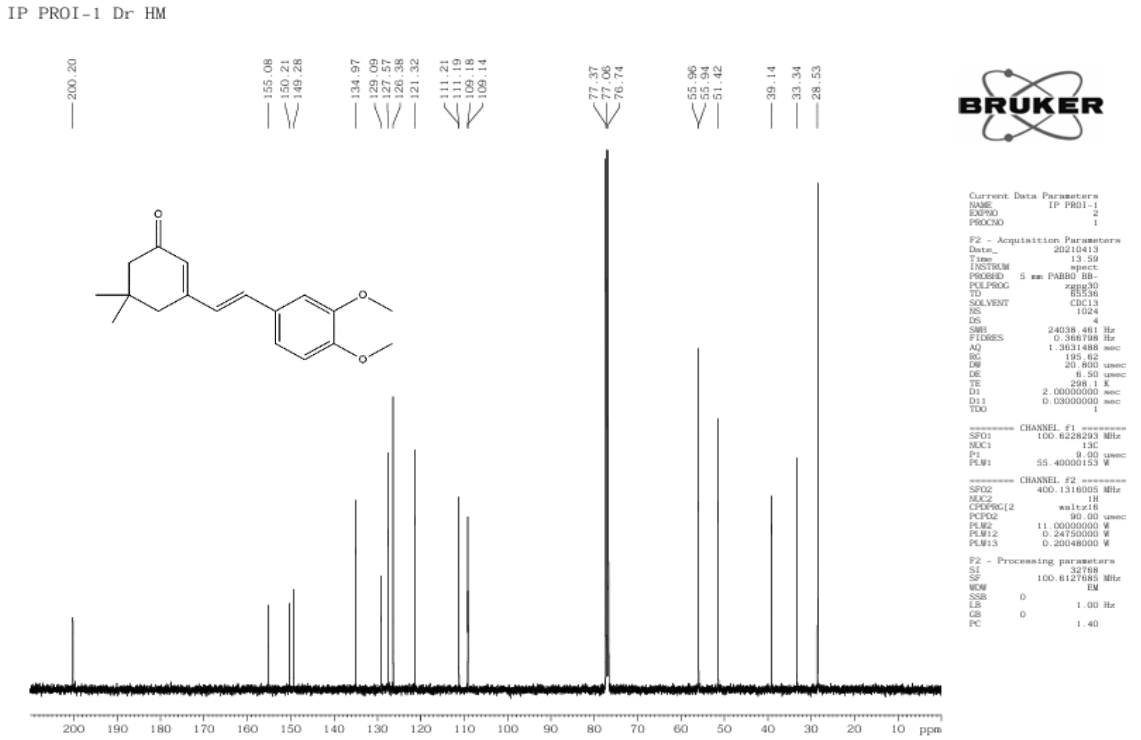

Figure 3. ^{13}C NMR spectrum of compound IPV.

the data integration using a monoclinic unit cell produced 22205 reflections in total, of which 4745 were independent (average redundancy 4.680, completeness = 98.3%, Rint = 7.34%, Rsig = 6.81%) and 1882 (39.66%) were larger than 2σ(F2). These are the parameters of the unit cell: a = 23.041(7) Å, b = 5.9791(19) Å and c = 11.743(3): α = 90°, β = 90.744(9)°, γ = 90°. The apparent transmission ratio was 0.735 from minimum to highest. According to crystal size, the lowest and maximum transmission coefficients are 0.9740 and 0.9820, respectively. With 194 variables, the final anisotropic full-matrix least-squares refinement on F2 converged at wR2 = 25.38% for all data and R1 = 8.29% for the observed data, the final difference electron density synthesis showed the biggest peak at 0.180 e-/Å3 and the largest hole at -0.209 e-/Å3. ORTEP and crystal packing of compound IPV as shown in the Figures 4 and 5. Table 2 provides a brief description of the compound's crystal and refinement data and their corresponding bond angle, bond lengths are given in Tables 3 and 4. The supplementary crystallographic data of IPV was CCDC NO. 2172927.

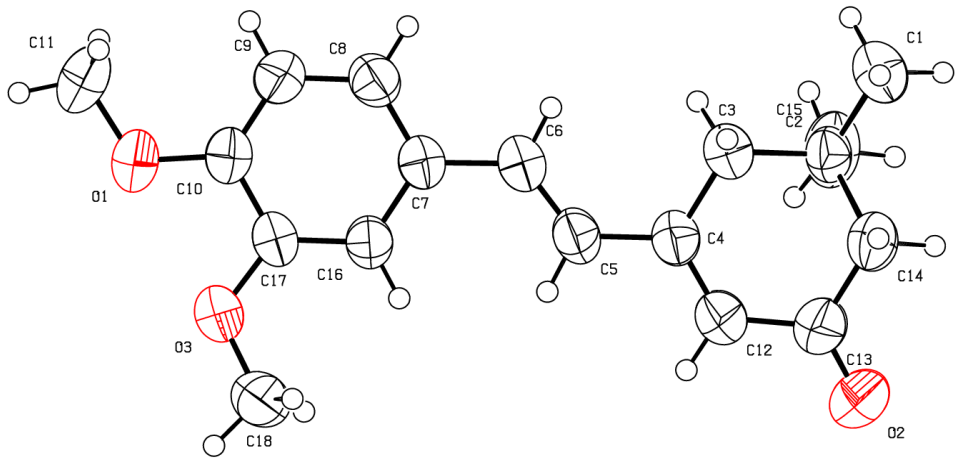

Figure 4. Ellipsoid plot ORTEP diagram of compound IPV.

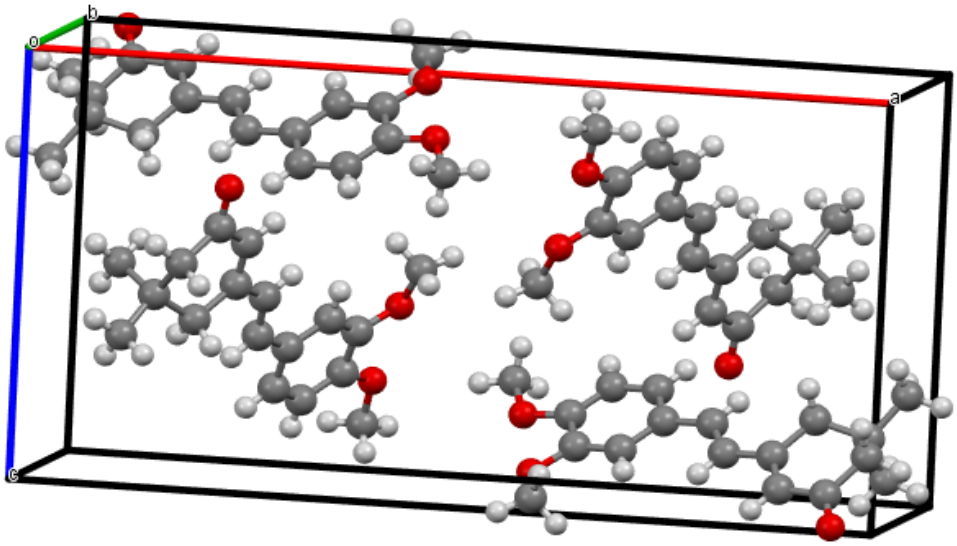

Figure 5. Packing diagram of compound IPV.

Table 2. Crystal and refinement data of compound IPV.

Identification code	DRHM_JSP1_16042021
Chemical formula	$C_{18}H_{22}O_3$
Formula weight	286.35 g/mol
Temperature	295(2) K
Wavelength	0.71073 Å
Crystal size	0.230 x 0.280 x 0.370 mm
Crystal system	monoclinic
Space group	P 1 21/c 1
Unit cell dimensions	a = 23.041(7) Å α = 90° b = 5.9791(19) Å β = 90.744(9)° c = 11.743(3) Å γ = 90°
Volume	1617.6(9) $Å^3$
Z	4
Density (calculated)	1.176 g/cm^3
Absorption coefficient	0.079 mm^{-1}
F(000)	616
Theta range for data collection	2.65 to 30.21°
Index ranges	-32<=h<=32, -8<=k<=8, -14<=l<=16
Reflections collected	22205
Independent reflections	4745 [R(int) = 0.0734]
Coverage of independent reflections	98.3%
Absorption correction	Multi-Scan
Max. and min. transmission	0.9820 and 0.9740
Structure solution technique	direct methods
Structure solution program	SHELXT 2014/5 (Sheldrick, 2014)
Refinement method	Full-matrix least-squares on F^2
Refinement program	SHELXL-2018/3 (Sheldrick, 2018)
Function minimized	$\Sigma w(F_o^2 - F_c^2)^2$
Data / restraints / parameters	4745 / 0 / 194
Goodness-of-fit on F^2	1.022
Largest diff. peak and hole	0.180 and -0.209 $eÅ^{-3}$
R.M.S. deviation from mean	0.042 $eÅ^{-3}$

Table 3. Bond lengths (Å) for compound IPV.

O1-C10	1.360(3)	O1-C11	1.417(4)
O2-C13	1.221(4)	O3-C17	1.369(3)
O3-C18	1.412(3)	C1-C2	1.534(4)
C1-H12	0.96	C1-H1	0.96
C1-H11	0.96	C2-C14	1.517(4)
C2-C15	1.518(4)	C2-C3	1.522(4)
C3-C4	1.512(4)	C3-H6	0.97
C3-H7	0.97	C4-C12	1.345(4)
C4-C5	1.436(4)	C5-C6	1.327(4)
C5-H14	0.93	C6-C7	1.452(3)
C6-H3	0.93	C7-C8	1.388(4)
C7-C16	1.402(3)	C8-C9	1.379(4)
C8-H19	0.93	C9-C10	1.370(4)
C9-H20	0.93	C10-C17	1.402(4)
C11-H22	0.96	C11-H21	0.96
C11-H2	0.96	C12-C13	1.444(4)
C12-H13	0.93	C13-C14	1.501(4)
C14-H4	0.97	C14-H5	0.97
C15-H8	0.96	C15-H10	0.96
C15-H9	0.96	C16-C17	1.365(3)
C16-H15	0.93	C18-H17	0.96
C18-H18	0.96	C18-H16	0.96

Table 4. Bond angles (°) for compound IPV.

C10-O1-C11	118.1(2)	C17-O3-C18	116.9(2)
C2-C1-H12	109.5	C2-C1-H1	109.5
H12-C1-H1	109.5	C2-C1-H11	109.5
H12-C1-H11	109.5	H1-C1-H11	109.5
C14-C2-C15	110.8(3)	C14-C2-C3	109.0(2)
C15-C2-C3	109.4(2)	C14-C2-C1	109.8(2)
C15-C2-C1	108.8(3)	C3-C2-C1	109.0(2)
C4-C3-C2	113.6(2)	C4-C3-H6	108.8
C2-C3-H6	108.8	C4-C3-H7	108.8
C2-C3-H7	108.8	H6-C3-H7	107.7
C12-C4-C5	120.2(3)	C12-C4-C3	120.1(2)
C5-C4-C3	119.6(2)	C6-C5-C4	127.7(3)
C6-C5-H14	116.1	C4-C5-H14	116.1
C5-C6-C7	127.1(3)	C5-C6-H3	116.5
C7-C6-H3	116.5	C8-C7-C16	117.7(2)
C8-C7-C6	120.1(2)	C16-C7-C6	122.3(2)
C9-C8-C7	121.3(2)	C9-C8-H19	119.4
C7-C8-H19	119.4	C10-C9-C8	120.7(3)
C10-C9-H20	119.6	C8-C9-H20	119.6
O1-C10-C9	125.8(2)	O1-C10-C17	115.3(2)
C9-C10-C17	118.8(2)	O1-C11-H22	109.5
O1-C11-H21	109.5	H22-C11-H21	109.5
O1-C11-H2	109.5	H22-C11-H2	109.5

H21-C11-H2	109.5	C4-C12-C13	123.9(3)
C4-C12-H13	118.0	C13-C12-H13	118.0
O2-C13-C12	122.0(3)	O2-C13-C14	121.8(3)
C12-C13-C14	116.1(3)	C13-C14-C2	114.1(2)
C13-C14-H4	108.7	C2-C14-H4	108.7
C13-C14-H5	108.7	C2-C14-H5	108.7
H4-C14-H5	107.6	C2-C15-H8	109.5
C2-C15-H10	109.5	H8-C15-H10	109.5
C2-C15-H9	109.5	H8-C15-H9	109.5
H10-C15-H9	109.5	C17-C16-C7	121.0(3)
C17-C16-H15	119.5	C7-C16-H15	119.5
C16-C17-O3	124.7(2)	C16-C17-C10	120.5(2)
O3-C17-C10	114.8(2)	O3-C18-H17	109.5
O3-C18-H18	109.5	H17-C18-H18	109.5
O3-C18-H16	109.5	H17-C18-H16	109.5
H18-C18-H16	109.5		

Hirshfeld Analysis, Fingerprint, Interaction Energies

Hirshfeld surface analysis was performed using Crystal Explorer 21 to examine weak intermolecular interactions in the crystal. CIF data from single-crystal XRD analysis helped visualize and quantify various intermolecular linkages. The dnorm surface plot highlights hydrogen bonding interactions, with bright red dots and dark red circles indicating significant fingerprint relationships. In dnorm mapping, the x-axis represents di (internal distance), while the y-axis represents de (external distance), with surfaces colored red (shorter than vdW radii), blue (longer), and white (equal to vdW radii).

The curvedness parameter describes surface curvature, where sharp curvatures indicate distinct molecular patches, while flat regions suggest minimal interaction. The shape index, shown as red and blue triangles, reveals π–π stacking interactions. The 2D fingerprint plot of IPV shows H···H contacts contributing 61.7 %, followed by ·O··H/H···O interactions concentrated at the edges. Other observed interactions include C···C, H···C, and C···H, as illustrated in Figures 6 and 7.

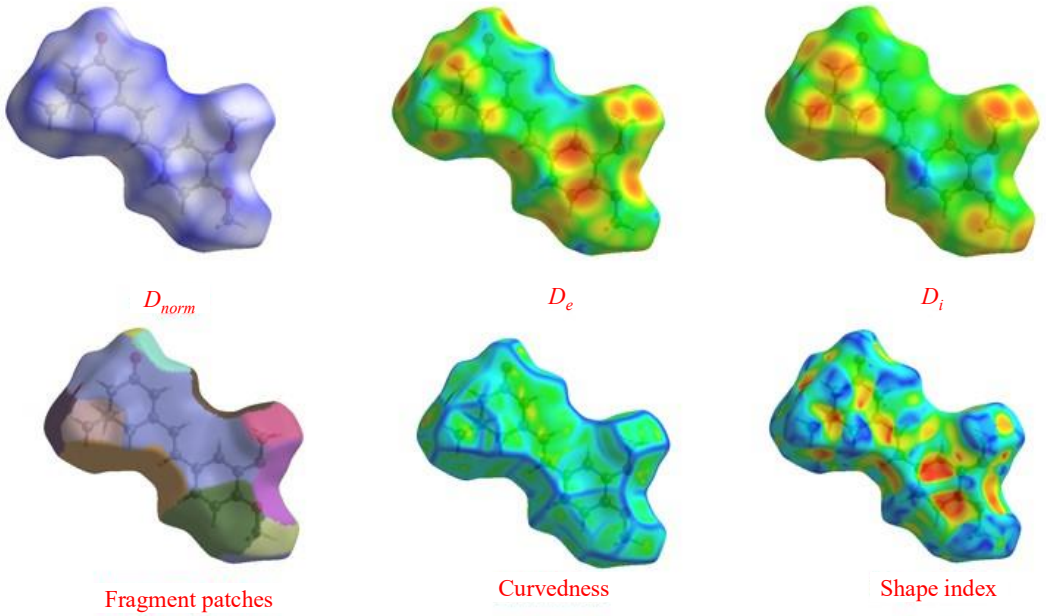

Figure 6. 3D Hirshfeld surface Analysis of compound IPV.

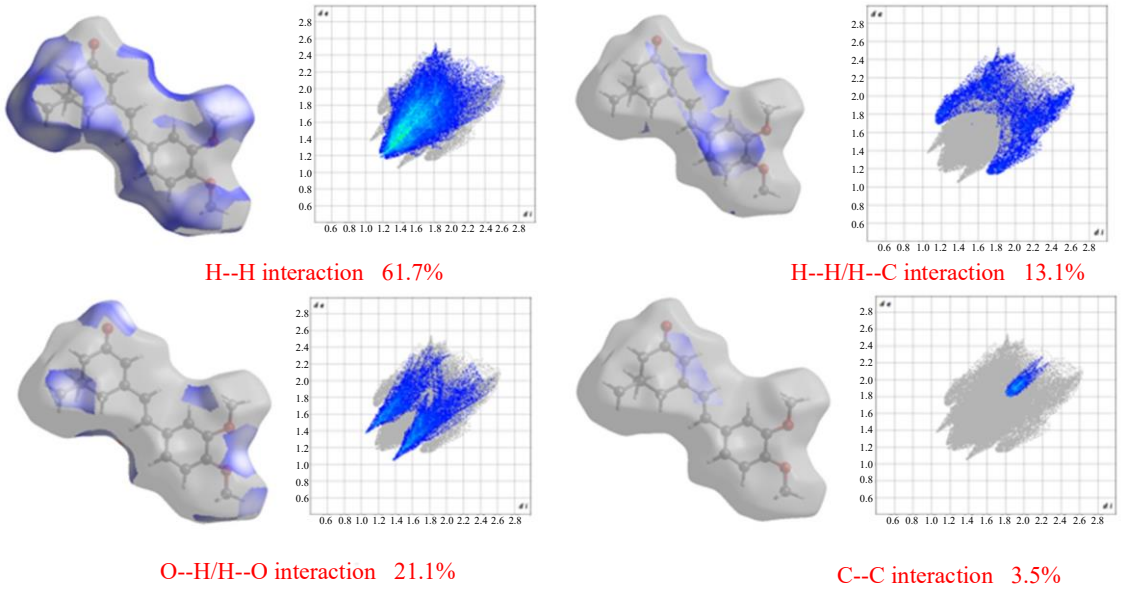

Figure 7. 2D-Fingerprint plot of compund IPV.

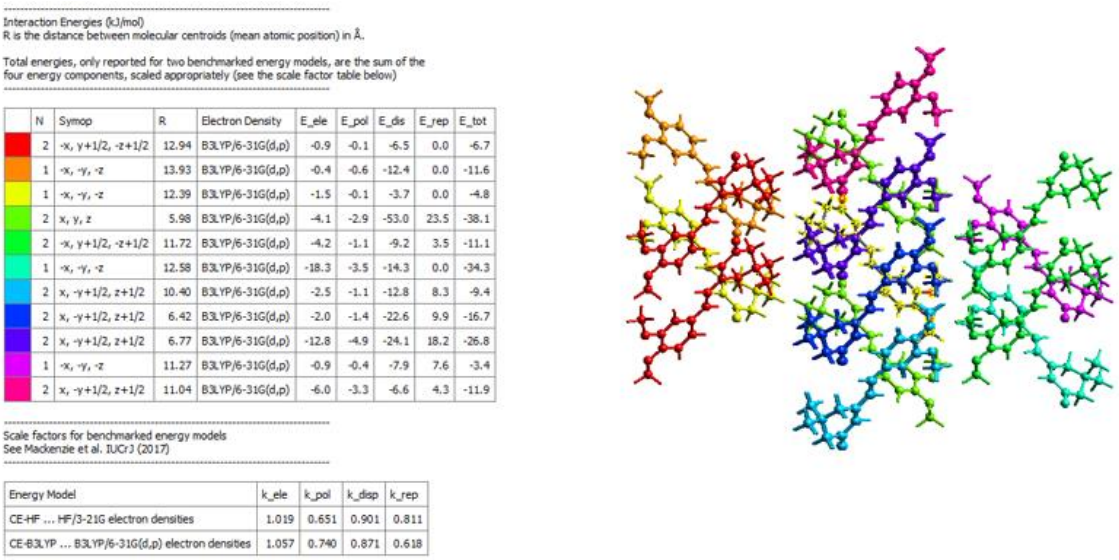

Interaction Energies (kJ/mol)
R is the distance between molecular centroids (mean atomic position) in Å.

Total energies, only reported for two benchmarked energy models, are the sum of the four energy components, scaled appropriately (see the scale factor table below)

	N	Symop	R	Electron Density	E_ele	E_pol	E_dis	E_rep	E_tot
	2	-x, y+1/2, -z+1/2	12.94	B3LYP/6-31G(d,p)	-0.9	-0.1	-6.5	0.0	-6.7
	1	-x, -y, -z	13.93	B3LYP/6-31G(d,p)	-0.4	-0.6	-12.4	0.0	-11.6
	1	-x, -y, -z	12.39	B3LYP/6-31G(d,p)	-1.5	-0.1	-3.7	0.0	-4.8
	2	x, y, z	5.98	B3LYP/6-31G(d,p)	-4.1	-2.9	-53.0	23.5	-38.1
	2	-x, y+1/2, -z+1/2	11.72	B3LYP/6-31G(d,p)	-4.2	-1.1	-9.2	3.5	-11.1
	1	-x, -y, -z	12.58	B3LYP/6-31G(d,p)	-18.3	-3.5	-14.3	0.0	-34.3
	2	x, -y+1/2, z+1/2	10.40	B3LYP/6-31G(d,p)	-2.5	-1.1	-12.8	8.3	-9.4
	2	x, -y+1/2, z+1/2	6.42	B3LYP/6-31G(d,p)	-2.0	-1.4	-22.6	9.9	-16.7
	2	x, -y+1/2, z+1/2	6.77	B3LYP/6-31G(d,p)	-12.8	-4.9	-24.1	18.2	-26.8
	1	-x, -y, -z	11.27	B3LYP/6-31G(d,p)	-0.9	-0.4	-7.9	7.6	-3.4
	2	x, -y+1/2, z+1/2	11.04	B3LYP/6-31G(d,p)	-6.0	-3.3	-6.6	4.3	-11.9

Scale factors for benchmarked energy models
See Mackenzie et al. IUCrJ (2017)

Energy Model	k_ele	k_pol	k_disp	k_rep
CE-HF ... HF/3-21G electron densities	1.019	0.651	0.901	0.811
CE-B3LYP ... B3LYP/6-31G(d,p) electron densities	1.057	0.740	0.871	0.618

Figure 8. Color-Color coded interaction map of IPV inside a 3.8*Å* cluster of molecules.

Intermolecular interaction energies were calculated and visualized using an energy framework to represent their magnitudes. Figure 8 illustrates the overall interaction energy of IPV.

DFT Studies

Figure 9 shows the optimized structure of obtained using the B3LYP/6-31(d,p) basis set, with atom numbering.

Frontier Molecular Orbital Approach

The frontier orbital theory suggests that the crystal exhibits chemical stability. The HOMO serves as both an electron donor and acceptor in the LUMO. The red and green hues represent the positive and negative phases, respectively [15–17]. The HOMO-LUMO energy gap for IPV is 3.3 eV, indicating high and consistent excitation energies. E_{HOMO} corresponds to the molecule's ionization energy, reflecting its ability to disperse electrons, while E_{LUMO} represents the molecule's electron affinity. The E_{HOMO}-E_{LUMO} energy gap determines whether a molecule is more inclined to donate or accept electrons.

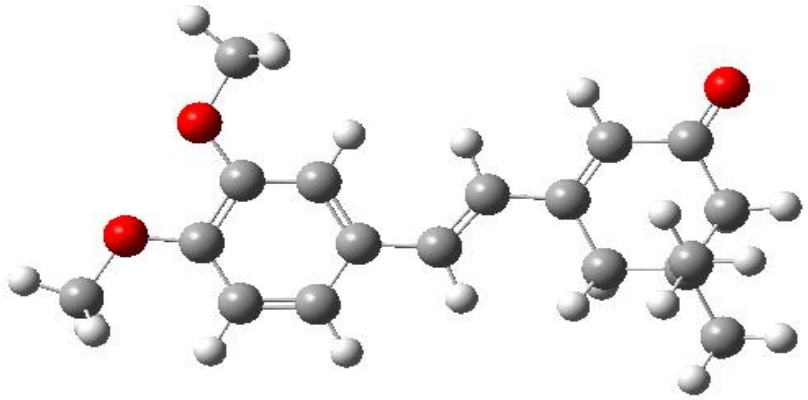

Figure 9. Optimized structure of compound IPV.

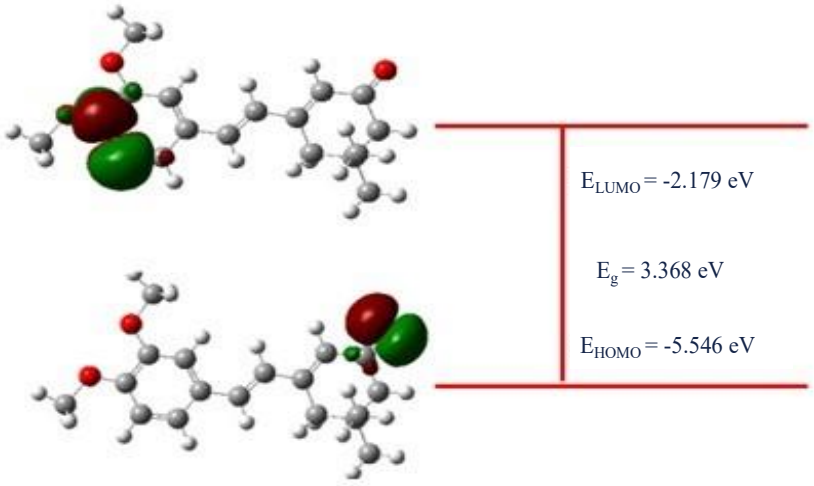

Figure 10. Frontier Molecular Orbital diagram of compound IPV.

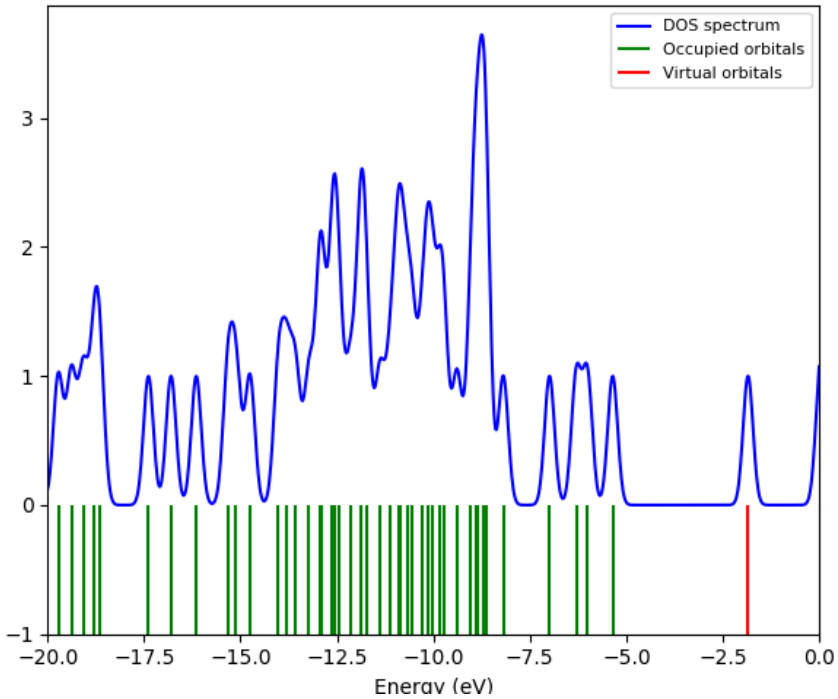

Figure 11. DOS diagram of IPV.

The HOMO-LUMO diagram provides a summary of these findings, illustrated in Figure 10. The fragmented HOMO-LUMO energy gap suggests that IPV is a promising material.

The DOS distribution diagram for synthesis compound was determined based on the optimized structure. Figure 11 illustrates the state spectrum density of the compound within the energy range of -15 to 10 eV, depicting the orbital geometries at various energy levels. Analysis of the DOS reveals that the energy gap for IPV is approximately 3.3 eV. In the diagram, red lines represent unoccupied molecular orbitals, while green lines denote occupied molecular orbitals.

Molecular Electrostatic Potential

Figure 12 presents a 3D MEP plot of compound, which is useful for analyzing nucleophilic and electrophilic reactivity. The negative regions (red) indicate electrophilic activity, while the positive regions (blue) correspond to nucleophilic activity [18, 19]. The molecular electrostatic potential across the molecule's surface is represented by a gradient of colors, ranging from deep red to deep blue in the order of red, orange, yellow, green, and blue. Blue signifies the strongest attraction, whereas red indicates the highest repulsion. The most electronegative atoms, primarily oxygen (O) and nitrogen (N), appear in red in Figure 7 highlighting their susceptibility to electrophilic attacks.

Mulliken Atomic Charge of IPV

Figures 13 and 14 illustrate the Mulliken atomic charge distribution of IPV, obtained using the B3LYP/6-311(d,p) method. Atoms with significant negative charges act as electron donors, while positively charged atoms serve as electron acceptors. Additionally, N or O-H atoms may facilitate the formation of intermolecular hydrogen bonds [20]. Table 5 illustrate the atomic charges analysis of compound IPV.

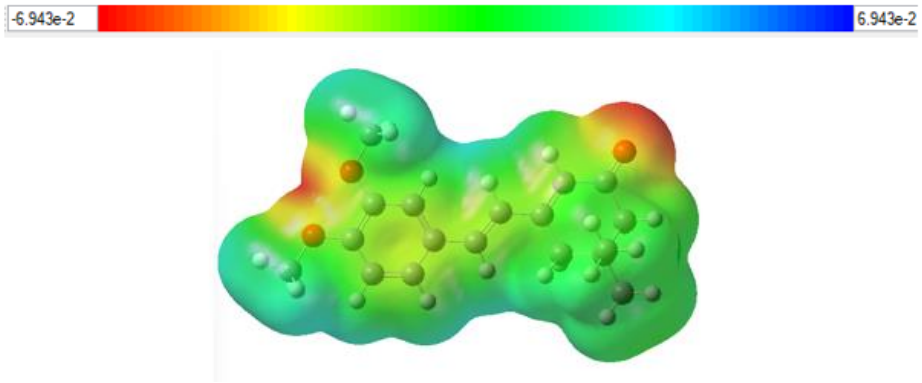

Figure 12. MEP diagram of IPV.

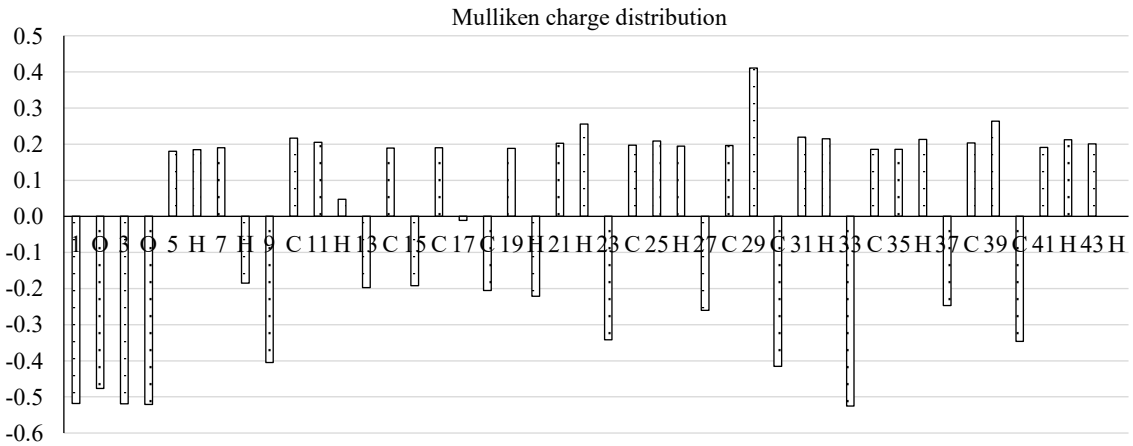

Figure 13. Mulliken atomic charge distribution bar diagram of compound.

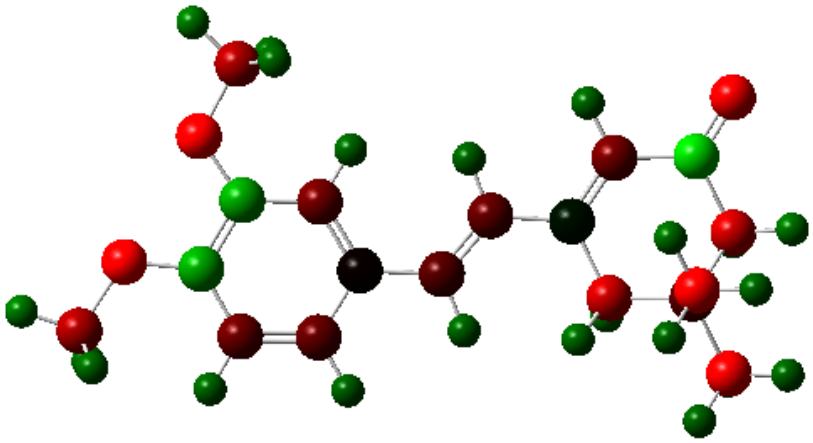

Figure 14. Mulliken atomic charge distribution diagram of compound.

Table 5. Mulliken atomic charge distribution of compound IPV.

1	O	-0.510566	21	H	0.206582
2	O	-0.469703	22	C	0.261438
3	O	-0.512986	23	C	-0.337806
4	C	-0.515019	24	H	0.203785
5	H	0.187432	25	H	0.217032
6	H	0.189628	26	H	0.198244
7	H	0.195080	27	C	-0.253648
8	C	-0.178036	28	H	0.199315
9	C	-0.401285	29	C	0.416582
10	H	0.221088	30	C	-0.412516
11	H	0.209163	31	H	0.226418
12	C	0.051792	32	H	0.221366
13	C	-0.190922	33	C	-0.519402
14	H	0.193961	34	H	0.191506
15	C	-0.187573	35	H	0.188492
16	H	0.196583	36	H	0.218242
17	C	-0.001951	37	C	-0.238159
18	C	-0.200026	38	H	0.208022
19	H	0.191056	39	C	0.268233
20	C	-0.212581	40	C	-0.338187

The Global Chemical Reactivity Descriptors Parameters (GCRD)

The following equations are used to derive the global chemical reactivity descriptor parameters, including Softness (S), Hyper-hardness (Γ), Electrophilicity index (ω), Electronegativity (X), and Dipole moment (μ) [19]. To assess a molecule's reactivity and stability, it is essential to consider its correlation with its structural properties.

$\Gamma = E_{LUMO}-2E_{HOMO}+E_{HOMO-I}$; $A= -E_{LUMO}$; $I= -E_{HOMO}$

$\omega = \mu^2/2\eta$; $X= -1/2\ (E_{HOMO}+E_{LUMO})$; $S= 1/2\ \eta$

$\eta =1/2\ (E_{LUMO}-E_{HOMO})$; $\mu=1/2\ (E_{LUMO}+E_{HOMO})$

Table 6 presents the calculated parameters of the GCRD values. The molecule's stability, in alignment with the chemical potential, is confirmed by the positive hyper-hardness value (12.26 eV). The global

Table 6. GCRD values.

Parameters	Calculated energies
Electronegativity (X)	-2.9
Hyper-hardness (Γ)	12.26
Electrophilicity index (ω)	-1.7
Chemical Softness (s)	-127.31
Chemical Hardness (η)	2.99
Ionization potential (I)	0.317
Electron affinity (A)	6.132

electrophilicity index (ω) values of 1.7 eV indicate weak electrophilic properties of the molecules. Additionally, the chemical hardness (η) value of 2.99 eV suggest activity within the IPV cavities, corresponding to the subsequent charge transfer process.

Atoms in Molecules and Non-covalent Interactions Reduced Density Gradient Analysis

AIM theory is a widely used approach for analyzing various types of chemical interactions and examining electron density at the bond ring critical point (RCP) of molecules. A key parameter derived from the first derivative of electron density is the reduced density gradient (RDG). Moderate intra- and intermolecular interactions play a crucial role in maintaining molecular structural stability. In this study, we employed the non-covalent interaction (NCI) method to investigate RDG. At the time of writing, the first derivative of electron density is:

$$RDG(r)=\frac{1}{2(3\pi^2)^{\frac{1}{3}}}\frac{|\nabla^{\rho}(r)|}{\rho(r)^{\frac{4}{3}}}$$

Intermolecular interactions were visualized in three dimensions using the NCI analysis method, as illustrated in Figure 15. The dashed red regions indicate repulsive interactions and steric effects occurring between the two aromatic rings. These interactions correspond to the red areas in the RDG plot, which signify π-π stacking interactions. Similarly, the presence of both red and green regions suggests atomic repulsion within the depicted area.

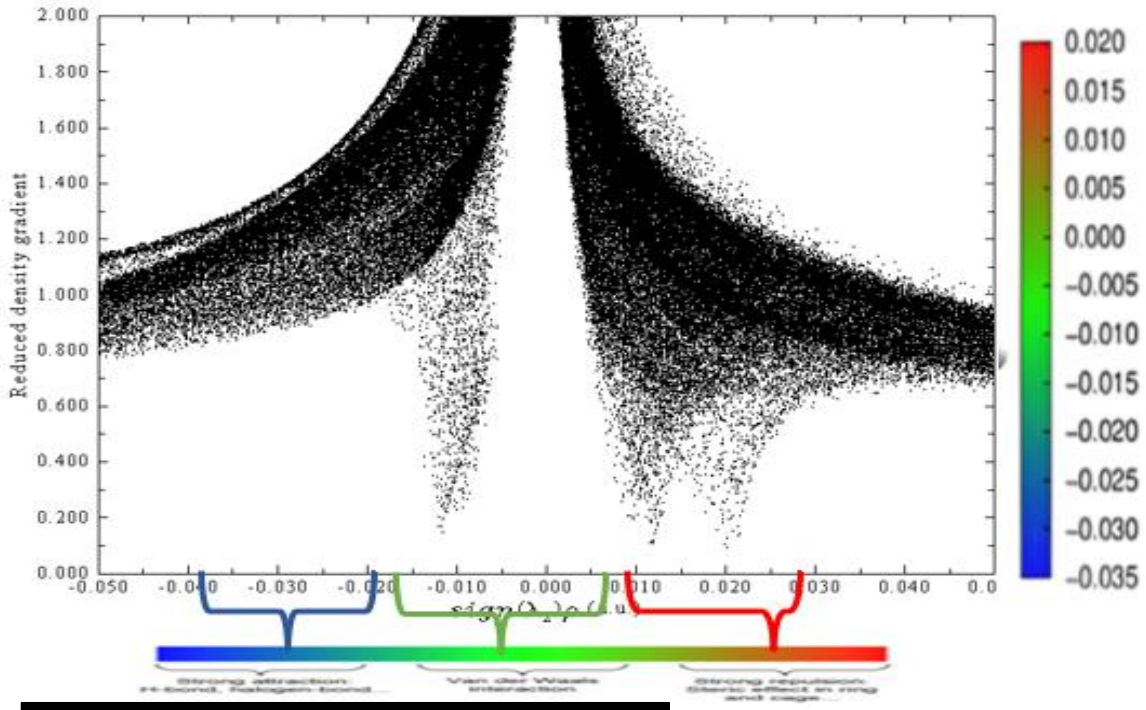

(a) Scatter Graph of compound IPV

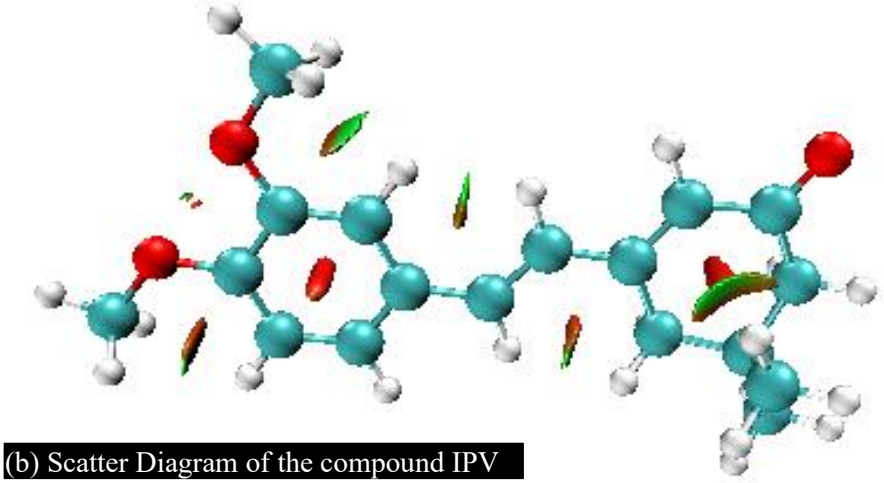

(b) Scatter Diagram of the compound IPV

Figure 15. Scatter graph and scatter diagram of the compound.

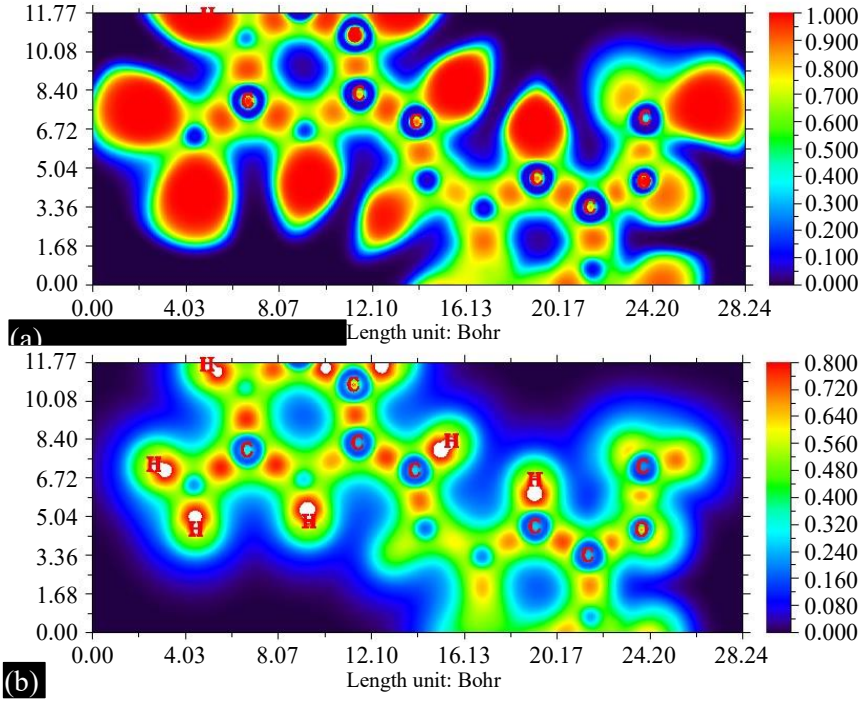

Figure 16. ELF and LOL representation of compound.

ELF and LOL

The LOL and ELF provide foundation for controlling the concentration of electron density [21]. Covalent bond analysis identifies regions of the chemical structure where a pair of electrons is more likely to be found. These functions are managed by Multiwfn 3.7 application. The mapping results from Multiwfn software for compound IPV are shown in Figure 16.

PHARMACOLOGICAL SCREENING

Antidiabetic Activity

The amylase enzyme inhibition technique was used to scrutinized the compound's antidiabetic properties using acarbose as a reference molecule Alpha-amylase inhibitors work by interfering with the enzyme's ability to hydrolyze starch into simple sugars. Standard and compound were prepared with different concentrations of 20, 40, 80, 200, and 400 µg/ml, respectively. As a result of the study, the compound have the α-amylase enzyme inhibition percentages almost nearer to standard one.

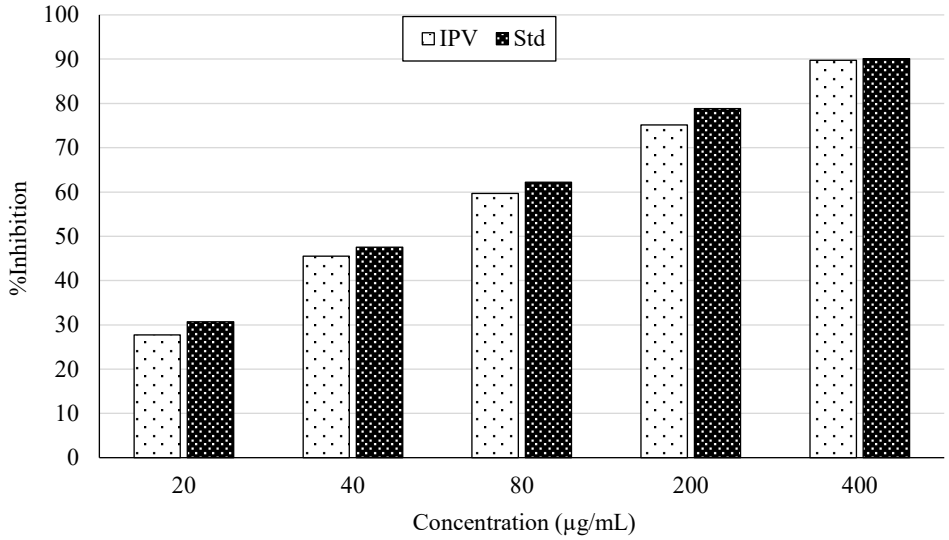

Figure 17. α-amylase enzyme inhibition of compound IPV.

Table 7. α- amylase enzyme inhibition of compound IPV.

Concentration	% Inhibition of IPV	% Inhibition of standard
20	27.75665	30.67174
40	45.50063	47.52852
80	59.69582	62.23067
200	75.15843	78.83397
400	89.73384	90.11407

The percentage of inhibition was calculated using the test and control data, and the various concentrations and their percentage of inhibitions were displayed in Figure 17 and Table 7. The results showed that the cyclohexenone moiety may have a major effect on α-amylase inhibition.

Anti-inflammatory Activity

Protein denaturation is a process that alters a protein's previous chemical structure and function. A number of external stimuli, including an acid, a base, a hazardous solvent, or any increased concentration of metal ions, might cause this denaturation. Therefore, it's a highly delicate process, and any small object may also interfere with the way a protein functions, which ultimately results in denaturation. Inflammation results from proteins losing their biological activity due to denaturation. The produced compound's anti-inflammatory activity against bovine serum albumin (BSA) was investigated as part of the study on the mechanism of the anti-inflammatory activity, and the outcomes were contrasted with those of standard drug molecules (diclofenac sodium). The data on anti-inflammatory action is displayed in a bar chart in Figure 18. At different concentrations (20, 40, 80, 200, and 400 µg/ml), results were compared to the reference drug. In general, the compound's anti-inflammatory properties are stronger than those of regular diclofenac sodium. Table 8 displayed the percentage of inhibition.

Anti-oxidant Activity

The Total Antioxidant Activity (TAA) test measures how efficiently antioxidants cooperate in a sample to prevent oxidative damage or neutralize free radicals. The antioxidant activity of these synthetic compounds was compared to that of regular vitamin C using the total antioxidant method. Each material's overall antioxidant capacity was examined at varying concentrations of 20, 40, 80, 200, and 400, respectively. A slightly lower level of inhibition was found when the compounds were compared to vitamin C. In addition to the various concentrations, Figure 19 and Table 9 display the percentage of inhibition, which is calculated from the control and test findings. The compounds' overall antioxidant activity was modest, and it was more consistent with that of conventional vitamin C.

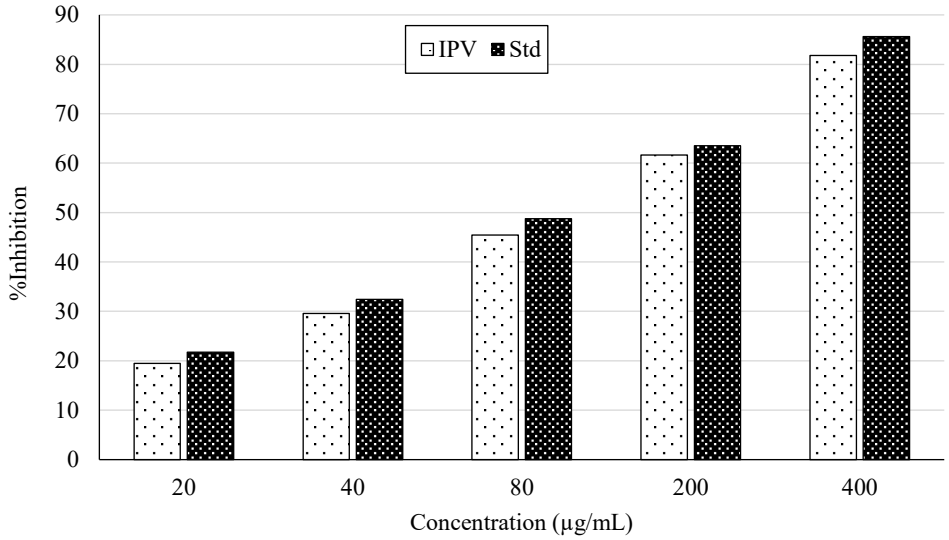

Figure 18. BSA Denaturation inhibition of compound IPV.

Table 8. BSA Denaturation inhibition of compound IPV

Concentration	% Inhibition of IPV	% Inhibition of Standard
20	19.46992864	21.7125382
40	29.56167176	32.4159021
80	45.46381244	48.72579
200	61.67176351	63.5066259
400	81.75331295	85.6269113

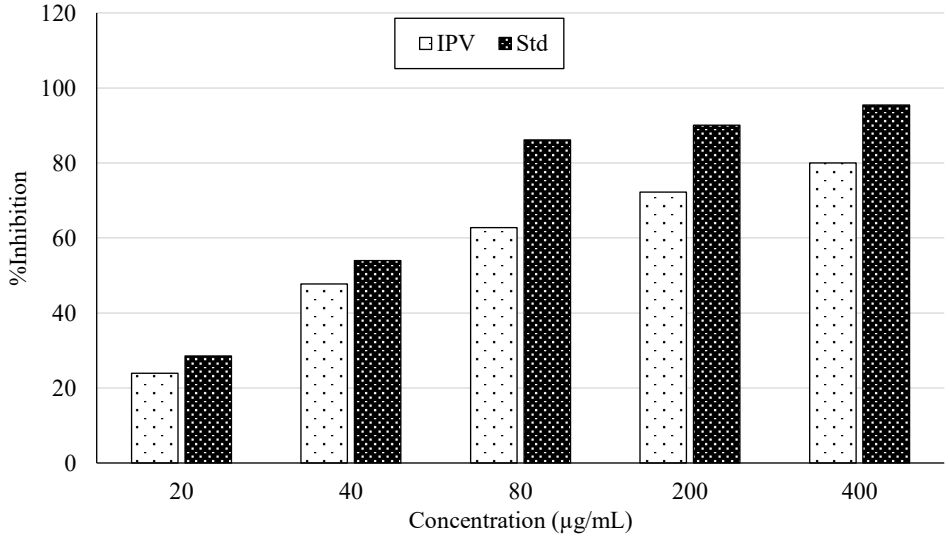

Figure 19. Total antioxidant activity of compound IPV.

Table 9. Total antioxidant activity of compound IPV

Concentration	% Inhibition of IPV	% Inhibition of Standard
20	23.91304	28.57143
40	47.76119	53.94737
80	62.76596	86.11111
200	72.22222	90.08499
400	80	95.43677

CONCLUSIONS

We report a new isophorone derivative 3-(3,4-dimethoxystyryl)-5,5-dimethylcyclohex-2-en-1-one molecule in this work that was synthesized by claisen Schmidt condensation and analysed by spectroscopic methods including FT-IR, ^{1}H NMR, ^{13}C NMR, and the X-ray diffraction structural approach. Additionally, B3LYP/6-31G (d,p) was used to optimize the geometrical properties of the compounds (d,p). Fingerprint plots, DFT, and Hirsch field surface analysis all offer compelling proof of the synthesized molecule's stability, intramolecular charge transfers, and donor-acceptor interactions. The nucleophilic and electrophilic areas of the molecule's surface were investigated using Mulliken atomic charges. The methoxy group's impact on aldehyde was a major finding. The methoxy group, as an electron donor, increases the electrophilicity of the aldehyde, making it more susceptible to nucleophilic attack by the enolate. This impact resulted in greater yields and faster reaction times when compared to reactions with non-methoxy substituted aldehydes. The methoxy group aided the preferential production of the trans-isomer of the isophorone derivative, as seen in the coupling constants in the ^{1}H-NMR spectrum. Additionally, the IPV molecules reveal exceptional pharmacological properties.

REFERENCES

1. Mojtahedi MM, Abaee MS, Zahedi MM, Jalali MR, Mesbah AW, Massa W, et al. Facile solvent-free synthesis and structural elucidation of styrylcyclohex-2-enone derivatives. Monatshefte Für Chem. 2008;139(8):917–21. https://doi.org/10.1007/s00706-007-0847-3
2. Eryilmaz S, Gül M, İnkaya E. Aldol türevi izoforan yapılarının sentezi, spektral karakterizasyonu, teorik analizi ve antioksidan aktiviteleri. Balıkesir Üniversitesi Fen Bilim Enstitüsü Derg. 2017:89–104. https://doi.org/10.25092/baunfbed.363772
3. Kasturi S, Surarapu S, Uppalanchi S, Anireddy JS, Dwivedi S, Anantaraju HS, et al. Synthesis and α-glucosidase inhibition activity of dihydroxy pyrrolidines. Bioorg Med Chem Lett. 2017;27(12):2818–23. https://doi.org/10.1016/j.bmcl.2017.04.078
4. Rafique R, Khan KM, Arshia, Kanwal, Chigurupati S, Wadood A, et al. Synthesis of new indazole based dual inhibitors of α-glucosidase and α-amylase enzymes, their in vitro, in silico and kinetics studies. Bioorg Chem. 2020;94:103195. https://doi.org/10.1016/j.bioorg.2019.103195
5. Mitra A. Mechanistic studies of lifestyle interventions in type 2 diabetes. World J Diabetes. 2012;3(12):201. https://doi.org/10.4239/wjd.v3.i12.201
6. Valko M, Rhodes CJ, Moncol J, Izakovic M, Mazur M. Free radicals, metals and antioxidants in oxidative stress-induced cancer. Chem Biol Interact. 2006;160(1):1–40. https://doi.org/10.1016/j.cbi.2005.12.009
7. El-Zahar M, Abd S, Anwar M, Danial E. Synthesis, antimicrobial and antioxidant activities of some novel cyclized naphthyl cyclohexanone derivatives. 2013.
8. Marchi S, Guilbaud E, Tait SWG, Yamazaki T, Galluzzi L. Mitochondrial control of inflammation. Nat Rev Immunol. 2023;23(3):159–73. https://doi.org/10.1038/s41577-022-00760-x
9. Wen X, Wang S-B, Liu D-C, Gong G-H, Quan Z-S. Synthesis and evaluation of the anti-inflammatory activity of quinoline derivatives. Med Chem Res. 2015;24(6):2591–603. https://doi.org/10.1007/s00044-015-1323-y
10. Logeshwari G, Jeyashri KR, Rajkumar M, Manikandan H, Sivakumar K, Selvanayagam S, et al. Benzylidene-isophorone hybrids with strong anticancer activity. Spectrochim Acta A Mol Biomol Spectrosc. 2024;319:124577. https://doi.org/10.1016/j.saa.2024.124577
11. Neela M, Premalatha B, Punitha P, Sabari Girisun TC. Synthesis, structural, third-order nonlinear optical properties and Hirshfeld surface analysis of 1-((E)-(4-chlorophenylimino)methyl)naphthalen-2-ol. Optik. 2023;290:171302. https://doi.org/10.1016/j.ijleo.2023.171302
12. Jeyashri K, Dhineshkumar E, Logeshwari G, Enbaraj E, Ramyadevi V, Manikandana H, et al. Design, synthesis of E-N-substituted-dichlorobenzylidene-2-(pyrrolidin-1-yl)ethanamine Schiff bases derivative and their DFT studies. IOP Conf Ser Mater Sci Eng. 2021;1070(1):012015. https://doi.org/10.1088/1757-899X/1070/1/012015

13. Sheldrick GM. SHELXT – integrated space-group and crystal-structure determination. Acta Crystallogr A Found Adv. 2015;71(1):3–8. https://doi.org/10.1107/S2053273314026370
14. Sheldrick GM. Crystal structure refinement with SHELXL. Acta Crystallogr C Struct Chem. 2015;71(1):3–8. https://doi.org/10.1107/S2053229614024218
15. Arulraj R. Hirshfeld surface analysis, interaction energy calculation and spectroscopical study of 3-chloro-3-methyl-r(2),c(6)-bis(p-tolyl)piperidin-4-one using DFT approaches. J Mol Struct. 2022;1248:131483. https://doi.org/10.1016/j.molstruc.2021.131483
16. Demir S, Cakmak S, Dege N, Kutuk H, Odabasoglu M, Kepekci RA. A novel 3-acetoxy-2-methyl-N-(4-methoxyphenyl)benzamide: molecular structural describe, antioxidant activity with use X-ray diffractions and DFT calculations. J Mol Struct. 2015;1100:582–91. https://doi.org/10.1016/j.molstruc.2015.08.014
17. Ramalingam A, Kansız S, Dege N, Sambandam S. Synthesis, crystal structure, DFT calculations and Hirshfeld surface analysis of 3-chloro-2,6-bis(4-chlorophenyl)-3-methylpiperidin-4-one. J Chem Crystallogr. 2021;51(2):273–87. https://doi.org/10.1007/s10870-020-00852-3
18. Albayati MR, Kansız S, Dege N, Kaya S, Marzouki R, Lgaz H, et al. Synthesis, crystal structure, Hirshfeld surface analysis and DFT calculations of 2-[(2,3-dimethylphenyl)amino]-N'-[(E)-thiophen-2-ylmethylidene]benzohydrazide. J Mol Struct. 2020;1205:127654. https://doi.org/10.1016/j.molstruc.2019.127654
19. Genç S, Dege N, Çetin A, Cansız A, Şekerci M, Dinçer M. 3-(2-Hydroxyphenyl)-4-phenyl-1H-1,2,4-triazole-5(4H)-thione. Acta Crystallogr E Struct Rep Online. 2004;60(9):o1580–2. https://doi.org/10.1107/S1600536804020367
20. Akter N, Bourougaa L, Ouassaf M, Bhowmic RC, Uddin KM, Bhat AR, et al. Molecular docking, ADME-Tox, DFT and molecular dynamics simulation of butyroyl glucopyranoside derivatives against DNA gyrase inhibitors as antimicrobial agents. J Mol Struct. 2024;1307:137930. https://doi.org/10.1016/j.molstruc.2024.137930
21. Subramaniyan R, Ramarajan R, Ramalingam A, Sambandam S, Petersamy A, Guerroudj AR, et al. Microwave assisted synthesis, vibrational spectra, Hirshfeld surface and interaction energy, DFT, topology, in silico ADMET and molecular docking studies of 1,2-bis(4-methoxybenzylidene)hydrazine. J Mol Struct. 2023;1278:134946. https://doi.org/10.1016/j.molstruc.2023.134946

